ARTICLE

doi:10.1038/nature11923

CLP1 links tRNA metabolism to progressive motor-neuron loss

Toshikatsu Hanada[1]*, Stefan Weitzer[1]*, Barbara Mair[1], Christian Bernreuther[2], Brian J. Wainger[3,4], Justin Ichida[5], Reiko Hanada[1], Michael Orthofer[1], Shane J. Cronin[3], Vukoslav Komnenovic[1], Adi Minis[6], Fuminori Sato[7], Hiromitsu Mimata[7], Akihiko Yoshimura[8], Ido Tamir[9], Johannes Rainer[10], Reinhard Kofler[10], Avraham Yaron[6], Kevin C. Eggan[5], Clifford J. Woolf[3,11], Markus Glatzel[2], Ruth Herbst[12], Javier Martinez[1] & Josef M. Penninger[1]

CLP1 was the first mammalian RNA kinase to be identified. However, determining its *in vivo* function has been elusive. Here we generated kinase-dead *Clp1* ($Clp1^{K/K}$) mice that show a progressive loss of spinal motor neurons associated with axonal degeneration in the peripheral nerves and denervation of neuromuscular junctions, resulting in impaired motor function, muscle weakness, paralysis and fatal respiratory failure. Transgenic rescue experiments show that CLP1 functions in motor neurons. Mechanistically, loss of CLP1 activity results in accumulation of a novel set of small RNA fragments, derived from aberrant processing of tyrosine pre-transfer RNA. These tRNA fragments sensitize cells to oxidative-stress-induced p53 (also known as TRP53) activation and p53-dependent cell death. Genetic inactivation of p53 rescues $Clp1^{K/K}$ mice from the motor neuron loss, muscle denervation and respiratory failure. Our experiments uncover a mechanistic link between tRNA processing, formation of a new RNA species and progressive loss of lower motor neurons regulated by p53.

RNA molecules undergo co- and post-transcriptional processing, leading to mature, functional RNAs. In mammals and archaea CLP1 proteins are kinases that phosphorylate the 5′ hydroxyl ends of RNA[1–3]. Human CLP1 is a component of the messenger RNA 3′-end cleavage and polyadenylation machinery[4,5], and studies in yeast have postulated a function for CLP1 in coupling mRNA 3′-end processing with RNA polymerase II (Pol II) transcriptional termination[6–8]. Unique to mammals is the association of CLP1 with the tRNA splicing endonuclease (TSEN) complex[9]. TSEN proteins remove the intron present within the anticodon loop of numerous pre-transfer RNAs (pre-tRNAs), generating 5′ and 3′ tRNA exon halves[10]. Within the TSEN complex, CLP1 phosphorylates 3′ tRNA exons *in vitro*[1], potentially contributing to tRNA splicing in mammals[11]. Although CLP1 may participate in multiple RNA pathways and was the first mammalian kinase identified that phosphorylates RNA, the *in vivo* function of CLP1 in mammalian cells has remained elusive.

We report the generation and phenotypic analysis of CLP1 kinase-dead mice. These mice develop a progressive loss of lower motor neurons, resulting in fatal deterioration of motor function. We also show that inactivation of CLP1 kinase activity results in the accumulation of previously unreported tyrosine tRNA fragments that sensitize cells to activation of p53 in response to oxidative stress.

Neonatal lethality of $Clp1^{K/K}$ mice

To assess the *in vivo* function of CLP1, first we generated global *Clp1*-knockout mice. We never obtained any viable *Clp1*-null offspring, even when analysed at embryonic day (E)6.5, indicating very early embryonic lethality. Consequently, we generated mice carrying a single amino-acid change, lysine to alanine at position 127 (K127A), which is located within the Walker A ATP-binding motif (Supplementary Fig. 1a, b). This mutation abolishes CLP1 kinase activity[1]. Mice heterozygous for the K127A substitution ($Clp1^{K/+}$) were intercrossed to generate homozygous offspring ($Clp1^{K/K}$). Western blotting showed that the CLP1 K127A mutant protein was expressed at normal levels, and that the $Clp1^{K/K}$ mutation impaired 5′ phosphorylation of a small duplex RNA substrate (Supplementary Fig. 1c, d). Therefore, we successfully generated a knock-in mouse expressing kinase-dead CLP1.

$Clp1^{K/K}$ mice were born at a normal Mendelian ratio. However, on a C57BL/6 background, all $Clp1^{K/K}$ mice died within hours of birth, probably owing to respiratory failure (Fig. 1a, b). This phenotype had complete penetrance ($n > 50$). Embryos and newborn $Clp1^{K/K}$ mice had overtly normal lung development and morphogenesis, as indicated by caveolin 1, surfactant A and surfactant C expression (Supplementary Fig. 2). However, all newborn $Clp1^{K/K}$ mice and E18.5 embryos exhibited a lordotic body posture and dropping forelimbs, indicative of impaired motor functions (Fig. 1a and Supplementary Fig. 3a). Newborn $Clp1^{K/K}$ mice also showed reduced birth weight and were hyporesponsive to stimuli (Supplementary Fig. 3b); similar phenotypes in KIF1B-mutant mice have been ascribed to motorsensory neuronal defects[12]. We therefore analysed neuromuscular junctions (NMJs) in the diaphragm.

Control E18.5 embryos showed the characteristic innervation pattern of the phrenic motor nerve bundle and had normal NMJs, defined by colocalization of presynaptic terminals with postsynaptic clusters of acetylcholine receptors (AChRs) as well as the presence of

[1]IMBA, Institute of Molecular Biotechnology of the Austrian Academy of Sciences, Vienna 1030, Austria. [2]Institute of Neuropathology, University Medical Center Hamburg-Eppendorf, Martinistrasse 52, Hamburg 20246, Germany. [3]Program in Neurobiology and F. M. Kirby Neurobiology Center, Boston Children's Hospital, Boston, Massachusetts 02115, USA. [4]Department of Anesthesia, Critical Care and Pain Medicine, Massachusetts General Hospital, Boston, Massachusetts 02114, USA. [5]Department of Stem Cell and Regenerative Biology, Howard Hughes Medical Institute, Harvard Stem Cell Institute. Boston, Massachusetts 02115, USA. [6]Department of Biological Chemistry. The Weizmann Institute of Science, Rehovot 76100, Israel. [7]Department of Urology, Oita University Faculty of Medicine, 1-1 Idaigaoka, Hasama-machi, Yufu, Oita 879-5593, Japan. [8]Department of Microbiology and Immunology, Keio University School of Medicine, Shinjuku-ku, Tokyo 160-8582, Japan. [9]Campus Science Support Facilities GmbH, Dr. Bohr-Gasse 3, Vienna 1030, Austria. [10]Division Molecular Pathophysiology, Biocenter, Medical University of Innsbruck, Innsbruck 6020, Austria. [11]Department of Neurobiology, Harvard Medical School, Boston, Massachusetts 02115, USA. [12]Center for Brain Research, Medical University of Vienna, Spitalgasse 4, Vienna 1090, Austria.
*These authors contributed equally to this work.

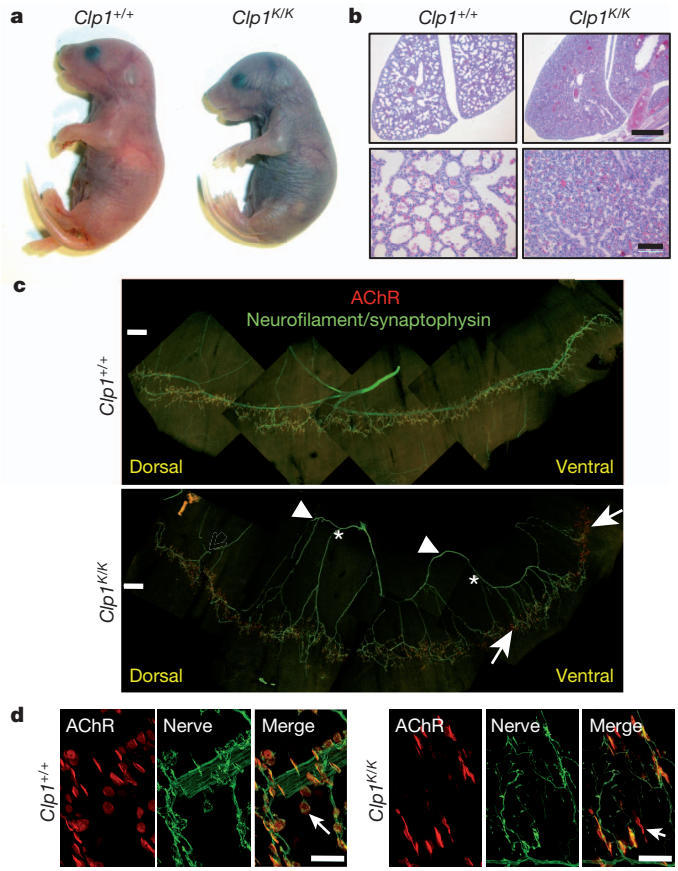

Figure 1 | Respiratory failure and impaired innervation of the diaphragm. **a**, **b**, Appearance (**a**) and lung histology (**b**; haematoxylin and eosin) of newborn *Clp1*$^{+/+}$ and *Clp1*$^{K/K}$ littermates on a C57BL/6 background. Scale bars: top, 500 μm; bottom, 100 μm. **c**, **d**, Whole-mount immunostaining of diaphragm muscle of E18.5 *Clp1*$^{+/+}$ and *Clp1*$^{K/K}$ littermates showing postsynaptic AChR clusters (red, α-bungarotoxin), and innervating motor axons and presynaptic nerve terminals (green, neurofilament/synaptophysin immunostaining). Asterisks indicate defasciculated main axons mislocalized to the periphery of the muscle; arrowheads indicate secondary branches coming from the main axon; arrows indicate areas of denervation. Magnifications in **d** indicate severely disturbed NMJs in E18.5 *Clp1*$^{K/K}$ embryos (arrow). Scale bars: **c**, 250 μm; **d**, 25 μm.

S100^{+} Schwann cells in the endplate (Fig. 1c and Supplementary Fig. 4). E18.5 *Clp1*$^{K/K}$ embryos showed defasciculation of the main phrenic nerve bundle; primary branches were mislocalized to the periphery, and denervation of the ventral and dorsal diaphragm was prominent in all *Clp1*$^{K/K}$ mutants (Fig. 1c). NMJs were formed, but axon terminals appeared undifferentiated, with smaller AChR clusters (Fig. 1d). S100 expression at the NMJ was absent in *Clp1*$^{K/K}$ embryos, although the Schwann cells seemed to be functionally intact as surviving peripheral axons were myelinated (Supplementary Fig. 4). The development and morphology of the heart, liver, kidney, colon, bladder, spleen and thymus appeared normal at E18.5. Thus, all newborn *Clp1*$^{K/K}$ mice show impaired innervation of the diaphragm, which seems to cause lethal respiratory failure and neonatal death.

Embryonic loss of motor neurons

We next assessed NMJs in the diaphragm during embryogenesis. In *Clp1*$^{K/K}$ embryos, denervation was not found at E14.5. However, we observed partial denervation and pronounced alteration in NMJ morphology at E16.5, followed by a severe defect in the innervation of the NMJs of the diaphragm at E18.5 (Fig. 1c, d and Supplementary Figs 4–6). Moreover, whereas *Clp1*$^{K/K}$ embryos had normal numbers of choline acetyl transferase (ChAT)-expressing spinal motor neurons at E14.5 and E16.5, the numbers of ChAT^{+} motor neurons markedly declined in the spinal cord of E18.5 *Clp1*$^{K/K}$ embryos (Fig. 2a, b and Supplementary Fig. 7a, b). The numbers of motor neurons also declined in wild-type embryos due to pruning, which has been linked to oxidative stress exposure[13]. NeuN staining to detect all neurons showed that the observed reduction in neuronal numbers was due to the loss of ChAT^{+} motor neurons (Supplementary Fig. 7c).

To confirm loss of motor neurons in the spinal cord, we crossed green fluorescent protein (GFP)-tagged Hb9 (also known as Mnx1) transgenic mice onto a *Clp1*$^{K/K}$ background. Genetic GFP tagging showed that E14.5 *Clp1*$^{K/K}$ embryos have similar numbers of Hb9^{+} cells as age-matched control embryos, but the numbers of Hb9–GFP^{+} cells declined in E18.5 *Clp1*$^{K/K}$ embryos (Supplementary Fig. 7d). In whole-mount visualizations of Hb9–GFP^{+} E10.5 embryos, both development and segmental-motor-axon outgrowth were comparable between *Clp1*$^{K/K}$ and control embryos; three-dimensional reconstructions further demonstrated comparable motor-axon outgrowth in the thoracic region (segment T6–T7) in E12.5 embryos

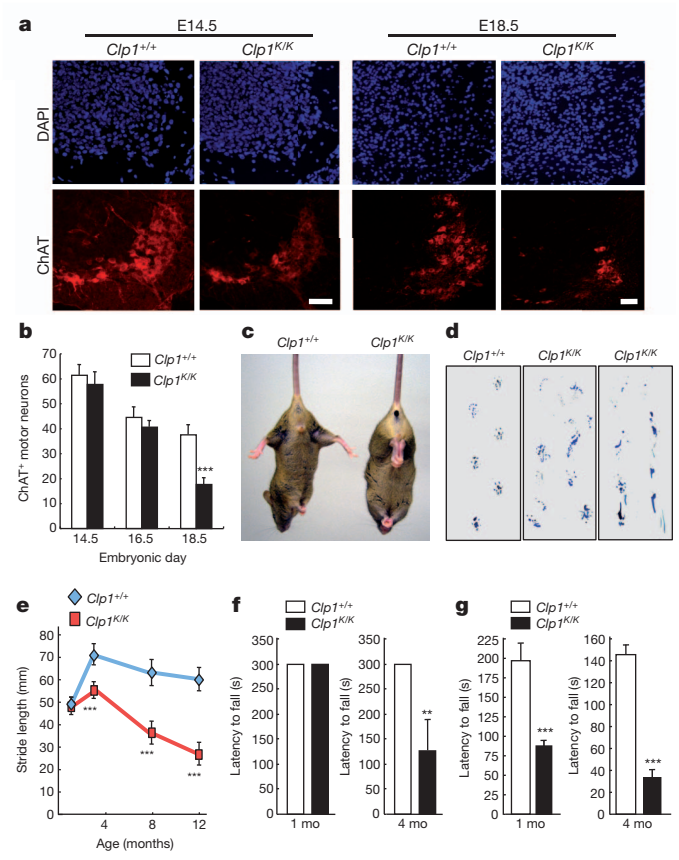

Figure 2 | Viable *Clp1*$^{K/K}$ embryos develop neuromuscular atrophy. **a**, Immunostaining for ChAT^{+} (red) motor neurons in the cervical (C4–C5) spinal cord of E14.5 and E18.5 *Clp1*$^{+/+}$ and *Clp1*$^{K/K}$ littermates on a C57BL/6 background. 4′,6-Diamidino-2-phenylindole (DAPI) staining is shown. Scale bar: 50 μm. **b**, Mean numbers ± standard deviation (s.d.) of ChAT^{+} motor neurons in the cervical (C4–C5) spinal cord of E14.5, E16.5 and E18.5 *Clp1*$^{+/+}$ and *Clp1*$^{K/K}$ littermates. $n = 5$ mice per group. $^{***}P < 0.001$ (*t*-test). **c**, Muscle weakness (impaired spreading of hind legs) in 3-month-old *Clp1*$^{K/K}$ mice. **d**, **e**, Impaired walking strides in 1-, 3-, 8- and 12-month-old *Clp1*$^{K/K}$ mice compared to *Clp1*$^{+/+}$ littermates. Representative images in **d** are from 12-month-old mice, demonstrating shortened walking strides and paralysis in *Clp1*$^{K/K}$ mice. Data in **e** are mean values ± s.d. $n = 5$ mice per group. $^{***}P < 0.001$ (*t*-test). **f**, **g**, Progressive impairment of motor functions in viable *Clp1*$^{K/K}$ mice as assessed by the latency to fall in a fixed (**f**) and accelerated (**g**) Rotarod test. Data (mean values ± s.d.) are from 1-month-old (mo) *Clp1*$^{+/+}$ ($n = 8$) and *Clp1*$^{K/K}$ ($n = 7$) mice, and 4-month-old *Clp1*$^{+/+}$ ($n = 16$) and *Clp1*$^{K/K}$ ($n = 14$) mice. $^{**}P < 0.01$, $^{***}P < 0.001$ (*t*-test).

(Supplementary Fig. 8a, b). Moreover, the overall morphology of motor terminal branches and the pathfinding of motor neurons at the intercostal muscles was comparable (Supplementary Fig. 8c). Thus, genetic inactivation of the RNA kinase function of CLP1 results in progressive loss of motor neurons in the cervical and lumbar spinal cord, with aberrant innervations and formation of NMJs in the diaphragm, and neonatal death.

Progressive loss of motor functions

The 100% lethality of *Clp1*$^{K/K}$ pups at birth was observed on a C57BL/6 background. Similarly, we observed 100% lethality on a BALB/c background. However, when crossing the mutation onto a CBA/J mouse background, we obtained viable pups homozygous for the *Clp1*$^{K/K}$ mutation (Supplementary Fig. 9a). These mice showed motor ataxia (Supplementary Fig. 9b), impaired muscle strength, an altered walking stride, and diminished balance as determined by the fixed and accelerated Rotarod tests (Fig. 2c–g), all indications of motor defects. The muscle weakness and impaired motor functions observed in these mice were progressive (Fig. 2e–g). Mice started to die around week 23 after birth, and older *Clp1*$^{K/K}$ mice developed limb paralysis (Fig. 2d and Supplementary Fig. 9a, c). Sensory responses to noxious heat, mechanical stimulation and capsaicin-induced pain appeared normal in *Clp1*$^{K/K}$ littermates (Supplementary Fig. 10).

Whereas *Clp1*$^{K/K}$ neonates on the CBA/J background had apparently normal numbers of spinal motor neurons, 4-month-old *Clp1*$^{K/K}$ mice showed both a marked reduction in ChAT^{+} and, as a second marker, SMI-32^{+} spinal motor neurons (Fig. 3a, b and Supplementary Fig. 11). The effects of the *Clp1* mutation on upper motor neurons need to be assessed. Consistent with lower motor neuron loss, we observed axonopathy of peripheral nerves such as the sciatic nerve (Fig. 3c, d and Supplementary Fig. 12a–c). Immunostaining showed amyloid-β precursor protein (APP)-positive structures, a marker for axonal injury[14], in the sciatic nerves of adult *Clp1*$^{K/K}$ mice (Fig. 3e). In line with motor-neuron loss, we observed a marked reduction in the number of large diameter (type 1A alpha) fibres, whereas the smaller sensory fibres were largely preserved (Supplementary Fig. 12d). Dorsal root ganglion (DRG) sensory neurons showed normal morphology and outgrowth. Whether developmental alterations in myelination also contribute to the phenotype needs to be further assessed. We also observed regional denervation and fragmentation of NMJs in the diaphragm, and in various limb and head skeletal muscles, resulting in skeletal muscle atrophy; slow-twitch muscles (soleus, gluteus) were less affected than the fast-twitch extensor digitorum longus or gastrocnemius muscles (Fig. 3f, g and Supplementary Figs 13–15). Similar results were obtained in SOD1 transgenic mice[15]. Thus, *Clp1*$^{K/K}$ mice develop progressive loss of spinal motor neurons and exhibit defective NMJs, resulting in impaired motor functions, muscular atrophy and limb paralysis.

CLP1 promotes efficient tRNA exon generation

To assess potential roles in RNA metabolic processes, first we evaluated the function of CLP1 in mRNA 3′-end cleavage[4]. The kinetics of a pre-mRNA cleavage reaction in nuclear extracts from wild-type and *Clp1*$^{K/K}$ mouse embryonic fibroblasts (MEFs) were similar (Supplementary Fig. 16a), suggesting that ATP binding and/or hydrolysis by CLP1 are dispensable for mRNA 3′-end cleavage. CLP1 has been implicated in RNA interference (RNAi) by its ability to phosphorylate small interfering RNAs *in vitro*[1]. We therefore assessed whether cellular microRNA (miRNA) processing or stability were affected by the CLP1 K127A mutation. However, the levels of various pre- and mature miRNAs did not differ between wild-type and *Clp1*$^{K/K}$ MEFs and tissues, and no effect on miRNA function was detected using a luciferase reporter assay (Supplementary Fig. 16b, c). Furthermore, we found no significant differences in pre-mRNA splicing (Supplementary Fig. 17).

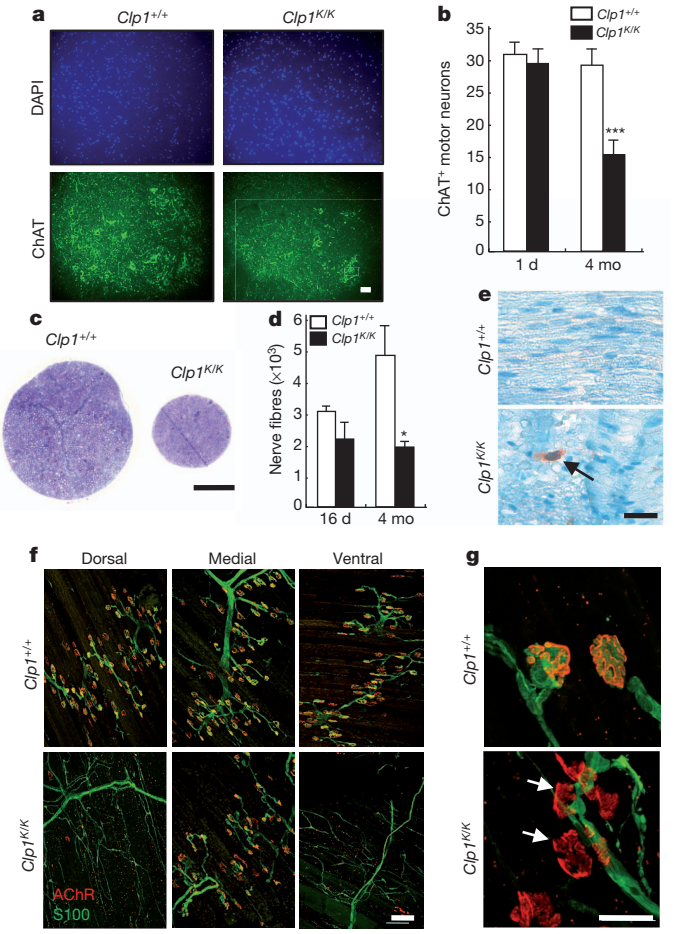

Figure 3 | Progressive loss of lower motor neurons. **a**, Immunostaining for ChAT^{+} (green) motor neurons in the lumbar (L5) spinal cord of 4-month-old *Clp1*$^{+/+}$ and *Clp1*$^{K/K}$ littermates on a CBA/J background. DAPI counterstaining. **b**, Mean numbers ± s.d. of ChAT^{+} motor neurons in the lumbar (L5) spinal cord of 1-day (d) and 4-month-old (mo) *Clp1*$^{+/+}$ and *Clp1*$^{K/K}$ littermates. $n = 5$ mice per group. ***$P < 0.001$ (*t*-test). **c**, Semi-thin cross-section of the sciatic nerve of 4-month-old *Clp1*$^{+/+}$ and *Clp1*$^{K/K}$ littermates. Toluidin blue staining. **d**, Mean numbers ± s.d. of total nerve fibres in the sciatic nerves of 16-day and 4-month-old *Clp1*$^{+/+}$ and *Clp1*$^{K/K}$ littermates. $n = 3$ mice per group. *$P < 0.05$ (*t*-test). **e**, Immunohistochemical detection of APP (arrow) in the sciatic nerve of a 12-month-old *Clp1*$^{K/K}$ mouse. **f**, **g**, Whole-mount immunostaining depicting NMJs in the diaphragms of 5-month-old *Clp1*$^{+/+}$ and *Clp1*$^{K/K}$ littermates. Postsynaptic AChR clusters are stained with α-bungarotoxin (red) and Schwann cells are labelled with anti-S100 antibodies (green). Arrows in **g** show NMJ fragmentations. Scale bars: **a**, 50 μm; **c**, 200 μm; **e**, 100 μm; **f**, 25 μm; **g**, 100 μm.

It has been reported that CLP1 is part of the human TSEN complex[9] and is able to phosphorylate tRNA 3′ exons[1]. We therefore tested whether the *Clp1*$^{K/K}$ mutation affects tRNA splicing. Notably, nuclear extracts from *Clp1*$^{K/K}$ MEFs generated significantly lower levels of tRNA exons (Fig. 4a). In addition, tRNA 3′ exon halves formed by incubation with nuclear extracts isolated from *Clp1*$^{K/K}$ MEFs lacked a 5′ phosphate group; 5′ phosphorylation and exon generation were rescued by ectopic expression of wild-type CLP1 in *Clp1*$^{K/K}$ MEFs (Supplementary Fig. 18a–e). Similarly, pre-tRNA cleavage was partially restored in *Clp1*$^{K/K}$ MEFs stably expressing wild-type CLP1, whereas overexpression of the CLP1 K127A mutant inhibited RNA phosphorylation (Supplementary Fig. 19a–d). Affinity-purified CLP1(K127A)-containing TSEN complexes were deficient in the generation of tRNA exons, most probably due to reduced levels of TSEN2, TSEN34 and TSEN54 subunits (Fig. 4b, c); mRNA levels of TSEN2, TSEN34 and TSEN54 were not affected in *Clp1*$^{K/K}$ MEFs (data not shown). Thus, the RNA kinase activity of CLP1 is important

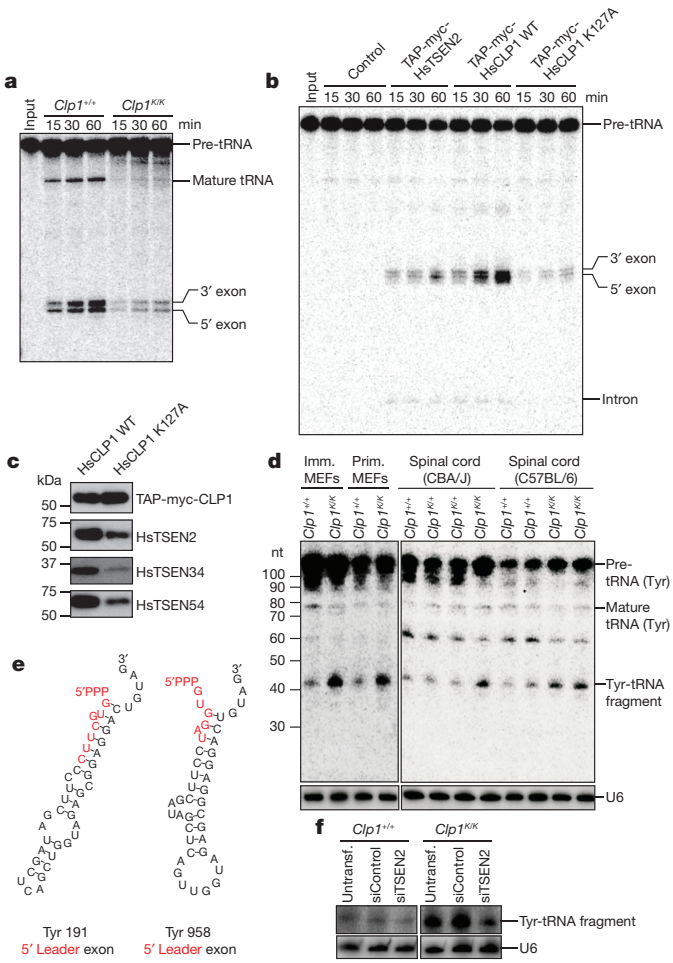

Figure 4 | Identification of a novel tRNA fragment. **a**, The RNA kinase activity of CLP1 is required for efficient tRNA exon generation *in vitro*. An internally labelled intron-containing yeast pre-tRNA^{Phe} was incubated with nuclear extracts from immortalized *Clp1*$^{+/+}$ and *Clp1*$^{K/K}$ MEFs. Pre-tRNA processing was monitored by electrophoresis. **b**, One-step purified human (Hs) TAP-myc-HsCLP1 (wild-type (WT) or K127A) and TAP-myc-HsTSEN2 complexes were assayed for pre-tRNA cleavage after elution with tobacco etch virus (TEV) protease (TEV eluate) by incubation with an internally labelled pre-tRNA^{Phe}. Eluates from HeLa cells expressing the vector without insert were used as control. **c**, The level of TSEN proteins in TAP-myc-HsCLP1 (wild type and K127A) TEV eluates was examined by western blot. Similar CLP1 protein levels were confirmed using anti-myc antibodies. **d**, ~41–46-nucleotide (nt) Tyr-tRNA fragments accumulate in primary (Prim.) and immortalized (Imm.) *Clp1*$^{K/K}$ MEFs and spinal cords of 4-month-old CBA/J *Clp1*$^{K/K}$ and newborn C57BL/6 *Clp1*$^{K/K}$ mice. Northern blot analyses of total RNA were performed with a DNA/LNA probe complementary to the 5′ exon of Tyr-tRNA. U6 RNA served as a loading control. **e**, Secondary structure of the two most abundant tRNA fragment species, Tyr-tRNA *M. musculus* chr14.trna191-TyrGTA and *M. musculus* chr13.trna958-TyrGTA (mouse July 2007 (mm9) genome assembly), as predicted by RNAfold (Vienna RNA Secondary Structure Package). **f**, Detection of Tyr-tRNA fragments from *Clp1*$^{+/+}$ and *Clp1*$^{K/K}$ MEFs left untransfected (Untransf.) or transfected with control siRNAs or siRNAs against TSEN2.

for the integrity of the TSEN complex and for efficient generation of tRNA exons (Supplementary Fig. 20).

Accumulation of novel tyrosine tRNA fragments

Whereas most tRNAs do not contain introns, all mouse tyrosine (Tyr)-tRNA genes contain an intronic sequence. Notably, in *Clp1*$^{K/K}$ MEFs we detected accumulation of ~41–46-nucleotide Tyr-tRNA fragments using a northern probe against the 5′ exon (Fig. 4d). RNA sequencing revealed that this fragment comprises a 5′ leader followed by 5′ exon Tyr-tRNA sequences (Fig. 4e and Supplementary Fig. 21a, b). Enzymatic treatments uncovered a 5′ triphosphate modification (Supplementary Fig. 21c), indicating that this novel tRNA fragment contains a full-length 5′ leader sequence starting with the transcription initiator PPP-nucleotide. RNAi-mediated silencing of TSEN2 in MEFs resulted in decreased levels of tRNA fragments (Fig. 4f and Supplementary Fig. 21d). Bioinformatic and northern blotting analyses revealed minor accumulation of such 5′ fragments from other intron-containing tRNAs, mostly arginine tRNAs (Supplementary Fig. 22).

A similar accumulation of tyrosine tRNA fragments was observed in the spinal cord of C57BL/6 *Clp1*$^{K/K}$ neonates and 4-month-old *Clp1*$^{K/K}$ mice on a CBA/J background (Fig. 4d). Moreover, we observed increased levels of these tRNA fragments in cortex, muscle, heart, kidney, muscle and liver (Supplementary Fig. 23a). Steady-state levels of mature tRNAs seemed to be normal in MEFs, the spinal cord of C57BL/6 *Clp1*$^{K/K}$ neonates and in postnatal CBA/J *Clp1*$^{K/K}$ mice (Supplementary Fig. 23b). Thus, loss of CLP1 kinase activity results in the accumulation of novel RNA fragments derived from pre-tRNA.

Oxidative-stress-induced cell death

Other tRNA fragments, for example, tRNA-derived, stress-induced small RNAs (tiRNAs), are generated in the cytoplasm by the endonuclease angiogenin acting on mature tRNAs[16,17]. Similar to tiRNAs, Tyr-tRNA fragments were also induced by H_2O_2, but were not generated by angiogenin. Rather, Tyr-tRNA fragments were present in the nucleus and were derived from pre-tRNAs actively transcribed by RNA Pol III (Supplementary Fig. 24a–d). Because Tyr-tRNA fragments were strongly induced by H_2O_2, we proposed that CLP1 might have a role in the oxidative stress response. In wild-type MEFs, the Tyr-tRNA fragments also accumulated after exposure to the reactive oxygen species (ROS) inducers glucose oxidase, menadione and paraquat dichloride, but not nefazodone (Supplementary Fig. 25a–d). Treatment with the mitochondrial 'poisons' carbonyl cyanide 4-(trifluoromethoxy) phenylhydrazone (FCCP) and rotenone, the apoptosis inducer staurosporine, the protein-synthesis inhibitor puromycin, and the DNA-damaging agent camptothecin did not trigger the accumulation of Tyr-tRNA fragments (Supplementary Fig. 25e, f). Importantly, on H_2O_2 and glucose oxidase challenge, we observed increased death of *Clp1*$^{K/K}$ MEFs; re-expression of wild-type CLP1 restored the survival rate to that of control MEFs (Fig. 5a and Supplementary Fig. 26a).

Extending our studies to neurons, we trans-differentiated wild-type and *Clp1*$^{K/K}$ MEFs into Hb9–GFP^{+} motor neurons[18], and observed typical sodium and potassium currents, as well as normal action potentials and responses to excitatory and inhibitory transmitters (Fig. 5b and Supplementary Fig. 26b–f). However, the resting membrane potential of *Clp1*$^{K/K}$ motor neurons was depolarized by over 10 mV relative to control motor neurons (-57.0 ± 2.0 mV for $n = 11$ *Clp1*$^{+/+}$ and -46.9 ± 3.0 mV for $n = 10$ *Clp1*$^{K/K}$ motor neurons; *t*-test <0.01), suggesting that *Clp1*$^{K/K}$ motor neurons exhibit ion-exchange abnormalities. Cell input resistance was similar between the two groups of neurons (367 ± 94 MΩ for $n = 11$ *Clp1*$^{+/+}$ and 511 ± 63 MΩ for $n = 10$ *Clp1*$^{K/K}$ motor neurons; *t*-test >0.2). Importantly, similar to MEFs, trans-differentiated *Clp1*$^{K/K}$ motor neurons were more sensitive to H_2O_2-induced cell death than wild-type motor neurons (Fig. 5c). Thus, loss of the catalytic activity of CLP1 results in enhanced motor-neuron death in response to oxidative stress.

Motor-neuron loss is mediated by p53

Oxidative stress has been linked to a p53-regulated cell death pathway through serine-18 phosphorylation, which has been shown to regulate p53-dependent transcription[19–21]. In response to H_2O_2, *Clp1*$^{K/K}$ MEFs showed hyperphosphorylation of p53 at serine 18 and increased induction of the p53-target gene p21 (also known as CDKN1A); re-expression of wild-type CLP1 rescued the H_2O_2-induced serine-18

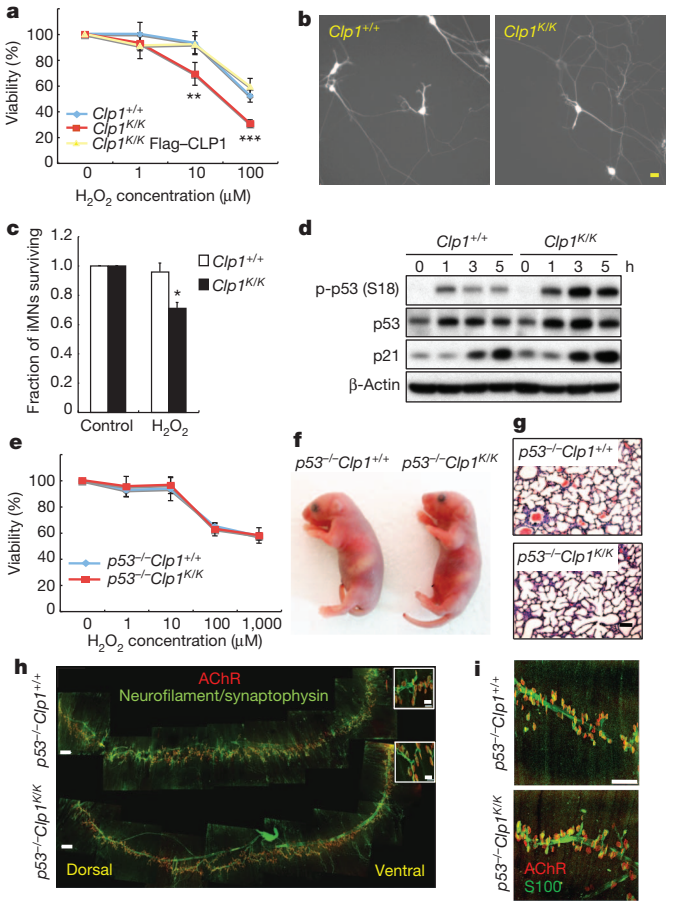

Figure 5 | Neonatal lethality and motor-neuron loss are mediated by p53. **a**, Viability of $Clp1^{+/+}$, $Clp1^{K/K}$ and $Clp1^{K/K}$ 3T3 MEFs rescued with Flag-tagged wild-type CLP1. Cells were exposed in triplicate to the indicated concentrations of H_2O_2 for 1 h, and mean viability was determined 12 h later. Data represent the means ± s.d. of three independent experiments. $^{**}P < 0.01$, $^{***}P < 0.001$ (analysis of variance (ANOVA)). **b**, Representative images of Hb9–GFP$^+$ trans-differentiated $Clp1^{+/+}$ and $Clp1^{K/K}$ motor neurons. Scale bar: 20 μm. **c**, Wild-type and $Clp1^{K/K}$ trans-differentiated motor neurons (iMNs) were treated in duplicate cultures with 100 μM H_2O_2 or water (control) for 3 h. Mean survival ± s.d. was scored after 48 h. $^{*}P < 0.05$ (paired *t*-test). **d**, p53 serine-18 phosphorylation (p) in H_2O_2-treated (100 μM for 1 h) $Clp1^{K/K}$ and $Clp1^{+/+}$ primary MEFs. Numbers indicate hours of recovery after stimulation. Time point 0 indicates no stimulation. β-Actin levels served as loading control. **e**, Mean viability ± s.d. of $p53^{-/-}Clp1^{+/+}$ and $p53^{-/-}Clp1^{K/K}$ MEFs challenged in triplicate with the indicated concentrations of H_2O_2 for 1 h. Cell viability was determined 12 h later. Data represent the means ± s.d. of three independent experiments. $^{*}P < 0.05$ (*t*-test). **f**, **g**, General appearance (**f**) and lung structures (**g**; haematoxylin and eosin) of newborn $p53^{-/-}Clp1^{+/+}$ and $p53^{-/-}Clp1^{K/K}$ littermates on a C57BL/6 background. Scale bar: 50 μm. **h**, Whole-mount immunostaining of the diaphragms of 3-day-old $p53^{-/-}Clp1^{+/+}$ and $p53^{-/-}Clp1^{K/K}$ littermates showing postsynaptic AChR clusters (red, α-bungarotoxin) and axons and branched presynaptic terminals of the phrenic nerve (green; neurofilament/synaptophysin immunostaining). Scale bar: 250 μm; inset: 25 μm. **i**, Whole-mount immunostaining of diaphragms of E18.5 $p53^{-/-}Clp1^{+/+}$ and $p53^{-/-}Clp1^{K/K}$ littermates showing postsynaptic AChR clusters (red; α-bungarotoxin) and Schwann cells (green; S100). Scale bar: 75 μm.

hyperphosphorylation (Fig. 5d and Supplementary Fig. 27a, b). Similarly, we found p53 serine-18 hyperphosphorylation in $Clp1^{K/K}$ MEFs in response to the ROS-inducing agent glucose oxidase but not the DNA-damaging agent camptothecin (Supplementary Fig. 27c, d). Most importantly, genetic inactivation of p53 rescued $Clp1^{K/K}$ MEFs from enhanced death after H_2O_2 treatment (Fig. 5e). Overexpression of two different tyrosine tRNA fragments in the mouse motor neuron cell line NSC-34 also resulted in enhanced p53 activation in response to H_2O_2 (Supplementary Fig. 28a, b). Thus, kinase-dead CLP1 renders MEFs more susceptible to oxidative-stress-induced cell death through a p53-regulated pathway.

Notably, we observed a complete rescue of neonatal lethality in $p53^{-/-}Clp1^{K/K}$ mice on the 100% lethal C57BL/6 background (Fig. 5f). The viable $p53^{-/-}Clp1^{K/K}$ pups showed normal extension of the lungs (Fig. 5g), normal innervation of the diaphragm, and rescue of NMJ formation (Fig. 5h, i). The numbers of ChAT- (Supplementary Fig. 29a, b) and SMI-32-labelled (data not shown) motor neurons in the spinal cord were comparable to that of newborn and 1-month-old control mice. Furthermore, 1-month-old $p53^{-/-}Clp1^{K/K}$ mice did not show muscle weakness (Supplementary Fig. 29c–e). Older $p53^{-/-}Clp1^{K/K}$ mice could not be assessed because they developed tumours due to the loss of p53. To test whether oxidative stress is involved in the phenotype, we treated pregnant $Clp1^{K/+}$ females (crossed to $Clp1^{K/+}$ males on the lethal C57BL/6 background) with the ROS scavenger *N*-acetylcysteine (NAC). NAC treatment resulted in viable $Clp1^{K/K}$ pups and partially restored innervation of the diaphragm (Supplementary Fig. 30). However, pups from NAC-treated mothers died within a week after birth, probably because *in vivo* ROS scavenging by NAC is incomplete and/or other pathways contribute to the phenotype. Thus, ROS and p53 constitute critical *in vivo* pathways that mediate motor neuronal loss and neonatal death of $Clp1^{K/K}$-mutant mice.

Transgenic rescue of motor-neuron defects

To provide definitive proof that the CLP1 kinase-dead mutation acts in motor neurons, we introduced a Flag-tagged wild-type CLP1-IRES-eGFP transgene under the control of the motor-neuron promoter Hb9 (ref. 22) into control and $Clp1^{K/K}$ mice on a C57BL/6 background (Fig. 6a and Supplementary Fig. 31a, b). Transgenic expression of wild-type CLP1 completely rescued neonatal lethality of $Clp1^{K/K}$ mice and restored normal numbers of ChAT$^+$ motor neurons in the spinal cord of newborns (Fig. 6b, c and Supplementary Fig. 31c). Moreover, Hb9-CLP1 transgenic $Clp1^{K/K}$ mice did not accumulate Tyr-tRNA fragments in the spinal cord (Fig. 6d), providing direct evidence that accumulation of these tRNA fragments is dependent on the loss of CLP1 activity. Phrenic nerve defasciculation and mislocalization, and the defects in NMJ formation and innervation of the diaphragm in $Clp1^{K/K}$ mice were also rescued by transgenic expression of wild-type CLP1 in $Clp1^{K/K}$ mice; similar results were obtained for intercostal muscles (Fig. 6e and Supplementary Fig. 32a–c). Moreover, S100$^+$ Schwann cells were restored (Fig. 6f), indicating that the observed absence of terminal Schwann cells is probably due to the impaired function of CLP1 in motor neurons.

Specific rescue of CLP1 expression in motor neurons but not other cell types led us to test whether kinase-dead CLP1 might affect general metabolism, which could then contribute to the observed phenotype. Using calorimetric experiments, $Clp1^{K/K}$ mice did not exhibit any apparent alterations in food and water intake, O_2 consumption, CO_2 production, respiratory exchange rate or heat generation as compared to the $Clp1^{+/+}$ transgenic littermates; moreover, heat generation upon cold exposure and recovery of body temperature, as a measure for sympathetic nerve activity[23], were comparable (Supplementary Fig. 33a–h). These transgenic rescue experiments provide direct evidence that CLP1 acts in lower motor neurons and that mutant-CLP1-mediated motor defects are responsible for the neonatal lethality phenotype.

Conclusions

Our results provide the first report on the *in vivo* function of the RNA kinase CLP1. CLP1 kinase-dead mice develop progressive loss of spinal motor neurons, leading to muscle denervation and paralysis. Inactivation of CLP1 kinase activity results at the same time in poor generation of tRNA exon halves and accumulation of novel, hitherto undescribed 5′ leader exon tRNA fragments. This paradoxical

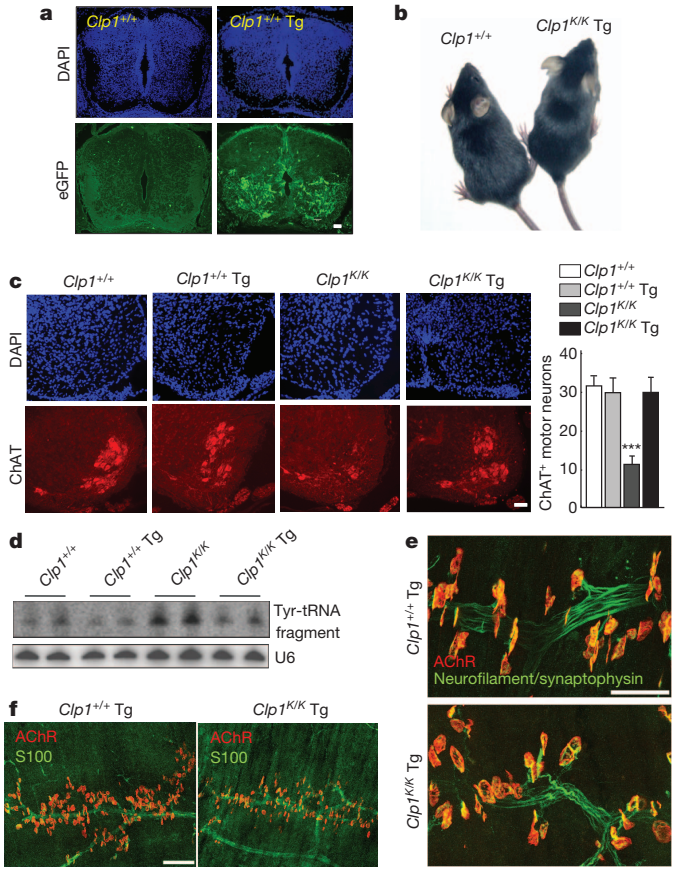

Figure 6 | CLP1 acts in motor neurons. **a**, Cryosections of lumbar (L5) spinal cord from E14.5 $Clp1^{+/+}$ and $Clp1^{+/+}$ Hb9-CLP1 transgenic ($Clp1^{+/+}$ Tg) embryos. Transgene expression was localized by eGFP and anti-GFP antibodies. DAPI counterstaining is shown. **b**, Appearance of 1-month-old $Clp1^{+/+}$ $Clp1^{K/K}$ transgenic littermates on a C57BL/6 background. **c**, Immunostaining for $ChAT^+$ (red) motor neurons in the lumbar (L5) spinal cord of newborn $Clp1^{+/+}$, $Clp1^{+/+}$ transgenic, $Clp1^{K/K}$ and $Clp1^{K/K}$ transgenic mice on a C57BL/6 background. DAPI staining. Right panel shows mean numbers ± s.d. of $ChAT^+$ motor neurons. $n = 5$ mice per group. $^{***}P < 0.001$ (ANOVA). **d**, Levels of Tyr-tRNA fragments in the spinal cord of $Clp1^{+/+}$, $Clp1^{+/+}$ transgenic, $Clp1^{K/K}$ and $Clp1^{K/K}$ transgenic mice. Northern blot analyses of total RNA using a probe complementary to the 5′ exon of Tyr-tRNA. U6 RNA served as a loading control. **e**, Whole-mount immunostaining depicting NMJs in diaphragms of 3-day-old $Clp1^{+/+}$ transgenic and $Clp1^{K/K}$ transgenic littermates. Postsynaptic AChR clusters (red; α-bungarotoxin) and innervating motor axons and presynaptic nerve terminals (green; neurofilament/synaptophysin immunostaining) are shown. **f**, Whole-mount immunostaining of the diaphragms of 3-day-old $Clp1^{+/+}$ transgenic, $Clp1^{K/K}$ and $Clp1^{K/K}$ transgenic littermates showing postsynaptic AChR clusters (red; α-bungarotoxin) and $S100^+$ Schwann cells (green). Scale bars: **a**, **c**, **e**, 50 μm; **f**, 100 μm.

observation could be explained by a defect in tRNA exon ligation in a CLP1 kinase-dead background regulated by oxidative stress. Different tRNA fragments have been previously reported in a variety of organisms[24,25]. For example, the cytoplasmatic pre-tRNA-derived tRF-1001 fragment, a 3′ trailer molecule, seems to have a role in cell viability[26]. Stress-induced tiRNAs, derived from the processing of mature tRNAs in the cytoplasm[16], inhibit initiation of protein translation by displacing the eIF4F complex from mRNAs[17]. We did not observe translation inhibition by our novel Tyr-tRNA fragments in metabolic labelling experiments; rather, we found that such fragments sensitize cells to oxidative-stress-induced activation of the p53 tumour suppressor pathway. The exact molecular mechanism(s) by which these tRNA fragments couple to the p53 pathway need to be determined. Importantly, motor-neuron loss was rescued *in vivo* either by reducing oxidative stress or by genetically inactivating p53.

Our experiments uncover an unexpected mechanistic link between tRNA processing, formation of a new RNA species, and a p53-regulated progressive loss of lower motor neurons. These results provide a conceptual and experimental framework for how alterations in tRNA metabolism can affect spinal motor neurons, and might help explain fundamental molecular principles in diseases such as amyotrophic lateral sclerosis or spinal muscular atrophy.

METHODS SUMMARY

Generation of kinase-dead $Clp1^{K/K}$ and Hb9-CLP1 transgenic mice. Complete mutant and knock-in $Clp1^{K/K}$ mice were generated by homologous recombination. The $Clp1^{K/K}$ allele was backcrossed five times to C57BL/6 or CBA/J mice. p53-deficient mice and Hb9–GFP transgenic mice were obtained from The Jackson Laboratory. Hb9-CLP1 transgenic mice containing the Hb9 promoter driving Flag-tagged mouse CLP1 and eGFP were generated in house. All mice were maintained according to institutional guidelines.

Phenotyping. Behavioural phenotyping and assessment of motor functions were performed as described in Supplementary Information. Diaphragm and intercostals muscles were stained as described previously[27]. Anti-neurofilament and anti-synaptophysin antibodies were used to label axons and presynaptic nerve terminals, respectively. Antibodies to S100 were used to visualize Schwann cells. Postsynaptic AChRs were detected with Alexa-594-conjugated α-bungarotoxin. Spinal motor neurons were stained with anti-ChAT and anti-SMI-32 antibodies. MEFs and trans-differentiated motor neurons were generated as described[18].

Pre-tRNA splicing. Pre-tRNA substrates were generated by *in vitro* transcription. Labelled yeast pre-$tRNA^{Phe}$ or human pre-$tRNA^{Tyr}$ were incubated with cell extracts or TEV eluates, and formation of mature tRNA and/or tRNA exons was monitored by phosphorimaging.

Northern blot analysis. For tRNA detection, total RNA from tissues and cultured cells was isolated, subjected to gel electrophoresis and blotted on Hybond-N^+ membranes. Blots were hybridized using [5′ ^{32}P]-labelled DNA/LNA probes to detect Tyr-tRNA 5′ and 3′ exons.

Identification of Tyr-tRNA fragments. Total RNA from primary MEFs was separated by gel electrophoresis. The region containing RNA of 37–50 nucleotides in size was excised and sequenced using an Illumina platform. Reads were aligned to the mouse genome (http://gtrnadb.ucsc.edu/Mmusc/Mmusc-by-locus-txt.html) using bedtools (v. 2.16.2).

Received 6 March 2012; accepted 18 January 2013.
Published online 10 March 2013.

1. Weitzer, S. & Martinez, J. The human RNA kinase hClp1 is active on 3′ transfer RNA exons and short interfering RNAs. *Nature* **447,** 222–226 (2007).
2. Ramirez, A., Shuman, S. & Schwer, B. Human RNA 5′-kinase (hClp1) can function as a tRNA splicing enzyme *in vivo*. *RNA* **14,** 1737–1745 (2008).
3. Jain, R. & Shuman, S. Characterization of a thermostable archaeal polynucleotide kinase homologous to human Clp1. *RNA* **15,** 923–931 (2009).
4. de Vries, H. *et al.* Human pre-mRNA cleavage factor II_m contains homologs of yeast proteins and bridges two other cleavage factors. *EMBO J.* **19,** 5895–5904 (2000).
5. Minvielle-Sebastia, L., Preker, P. J., Wiederkehr, T., Strahm, Y. & Keller, W. The major yeast poly(A)-binding protein is associated with cleavage factor IA and functions in premessenger RNA 3′-end formation. *Proc. Natl Acad. Sci. USA* **94,** 7897–7902 (1997).
6. Holbein, S. *et al.* The P-loop domain of yeast Clp1 mediates interactions between CF IA and CPF factors in pre-mRNA 3′ end formation. *PLoS ONE* **6,** e29139 (2011).
7. Haddad, R. *et al.* An essential role for Clp1 in assembly of polyadenylation complex CF IA and Pol II transcription termination. *Nucleic Acids Res.* **40,** 1226–1239 (2012).
8. Ghazy, M. A. *et al.* The interaction of Pcf11 and Clp1 is needed for mRNA 3′-end formation and is modulated by amino acids in the ATP-binding site. *Nucleic Acids Res.* **40,** 1214–1225 (2012).
9. Paushkin, S. V., Patel, M., Furia, B. S., Peltz, S. W. & Trotta, C. R. Identification of a human endonuclease complex reveals a link between tRNA splicing and pre-mRNA 3′ end formation. *Cell* **117,** 311–321 (2004).
10. Trotta, C. R. *et al.* The yeast tRNA splicing endonuclease: a tetrameric enzyme with two active site subunits homologous to the archaeal tRNA endonucleases. *Cell* **89,** 849–858 (1997).
11. Zillmann, M., Gorovsky, M. A. & Phizicky, E. M. Conserved mechanism of tRNA splicing in eukaryotes. *Mol. Cell. Biol.* **11,** 5410–5416 (1991).
12. Zhao, C. *et al.* Charcot-Marie-Tooth disease type 2A caused by mutation in a microtubule motor KIF1Bβ. *Cell* **105,** 587–597 (2001).
13. Sánchez-Carbente, M. R., Castro-Obregon, S., Covarrubias, L. & Narvaez, V. Motoneuronal death during spinal cord development is mediated by oxidative stress. *Cell Death Differ.* **12,** 279–291 (2005).
14. Medana, I. M. & Esiri, M. M. Axonal damage: a key predictor of outcome in human CNS diseases. *Brain* **126,** 515–530 (2003).
15. Atkin, J. D. *et al.* Properties of slow- and fast-twitch muscle fibres in a mouse model of amyotrophic lateral sclerosis. *Neuromuscul. Disord.* **15,** 377–388 (2005).

16. Yamasaki, S., Ivanov, P., Hu, G. F. & Anderson, P. Angiogenin cleaves tRNA and promotes stress-induced translational repression. *J. Cell Biol.* **185,** 35–42 (2009).
17. Ivanov, P., Emara, M. M., Villen, J., Gygi, S. P. & Anderson, P. Angiogenin-induced tRNA fragments inhibit translation initiation. *Mol. Cell* **43,** 613–623 (2011).
18. Son, E. Y. *et al.* Conversion of mouse and human fibroblasts into functional spinal motor neurons. *Cell Stem Cell* **9,** 205–218 (2011).
19. Lambert, P. F., Kashanchi, F., Radonovich, M. F., Shiekhattar, R. & Brady, J. N. Phosphorylation of p53 serine 15 increases interaction with CBP. *J. Biol. Chem.* **273,** 33048–33053 (1998).
20. Dumaz, N. & Meek, D. W. Serine 15 phosphorylation stimulates p53 transactivation but does not directly influence interaction with HDM2. *EMBO J.* **18,** 7002–7010 (1999).
21. Chao, C. *et al.* Cell type- and promoter-specific roles of Ser18 phosphorylation in regulating p53 responses. *J. Biol. Chem.* **278,** 41028–41033 (2003).
22. Arber, S. *et al.* Requirement for the homeobox gene *Hb9* in the consolidation of motor neuron identity. *Neuron* **23,** 659–674 (1999).
23. Hanada, R. *et al.* Neuromedin U has a novel anorexigenic effect independent of the leptin signaling pathway. *Nature Med.* **10,** 1067–1073 (2004).
24. Tuck, A. C. & Tollervey, D. RNA in pieces. *Trends Genet.* **27,** 422–432 (2011).
25. Hurto, R. L. Unexpected functions of tRNA and tRNA processing enzymes. *Adv. Exp. Med. Biol.* **722,** 137–155 (2011).
26. Lee, Y. S., Shibata, Y., Malhotra, A. & Dutta, A. A novel class of small RNAs: tRNA-derived RNA fragments (tRFs). *Genes Dev.* **23,** 2639–2649 (2009).
27. Herbst, R., Iskratsch, T., Unger, E. & Bittner, R. E. Aberrant development of neuromuscular junctions in glycosylation-defective *Large*^{myd} mice. *Neuromuscul. Disord.* **19,** 366–378 (2009).

Supplementary Information is available in the online version of the paper.

Acknowledgements We thank A. Meixner, M. Foong, T. Nakashima, H. C. Theussl, J. R. Wojciechowski, A. Bichl, the mouse pathology unit of the Universitätsklinikum Hamburg-Eppendorf, and G. P. Resch for discussions and technical support. We also thank T. Buerckstuemmer for providing the pRV-NTAP vector. J.M.P. is supported by grants from the Institute of Molecular Biotechnology of the Austrian Academy of Sciences (IMBA), the Austrian Ministry of Sciences, the Austrian Academy of Sciences, AustroMouse network of Genome Research in Austria (GEN-AU), Apoptosis systems biology applied to cancer and AIDS (ApoSys) and a European Research Council Advanced Grant from the European Union. J.M., S.W. and B.M. are supported by IMBA and GEN-AU (AustroMouse). T.H. is supported by the Japan Society for the Promotion of Science and the Astellas Foundation. J.K.I. was supported by National Institutes of Health (NIH) grant K99NS077435-01A1. M.G. is supported by grants from the German Research Foundation (DFG) (FG885 and GRK 1459), the Landesexzellenzinitiative Hamburg (Neurodapt). R.H. was supported by the Austrian Science Fund (P19223, P21667). C.J.W. is supported by the NIH (NS038253).

Author Contributions T.H. generated mutant mice, performed mouse phenotyping and developed cell lines with help from R.H. S.W. and B.M. performed all biochemical assays and northern blots. V.K. performed histological analysis. F.S., H.M., S.J.C. and A.Y. provided key reagents and technical help for generation of mutant mice. I.T. analysed tRNA fragment distributions. M.O. performed calorimetric experiments. B.J.W., J.I., K.C.E. and C.J.W. performed and helped with transdifferentiation experiments and patch clamping. R.H. performed immunostainings and assessment of NMJs and motor-neuron pathfinding. A.M. and A.Y. performed DRG explant cultures, and J.R. and R.K. carried out exon arrays. C.B. and M.G. performed histological and immunohistochemical staining of, and assessed, peripheral nerve and brain structures. J.M. and J.M.P. coordinated the project and wrote the manuscript.

Author Information Data have been deposited in the Gene Expression Omnibus under accession numbers GSE35924 and GSE39275. Reprints and permissions information is available at www.nature.com/reprints. The authors declare no competing financial interests. Readers are welcome to comment on the online version of the paper. Correspondence and requests for materials should be addressed to J.M. (javier.martinez@imba.oeaw.ac.at) or J.M.P. (josef.penninger@imba.oeaw.ac.at).